

Solving the fully non-linear weakly dispersive Serre equations for flows over dry beds.

J.P.A. Pitt^{a,*}, C. Zoppou^a, S.G. Roberts^a

^a*Mathematical Sciences Institute, Australian National University, Canberra, ACT 0200, Australia*

Abstract

We describe a numerical method for solving the Serre equations that can model flows over dry bathymetry. The method solves the Serre equations in conservation law form with a finite volume method. A finite element method is used to solve the auxiliary elliptic equation for the depth-averaged horizontal velocity. The numerical method is validated against the lake at rest analytic solution, demonstrating that it is well-balanced. The method is further validated and its convergence rate established using forced solutions containing the wetting and drying of bathymetry. The use of forced solutions extends previous validations performed for Serre equation solvers for flows over dry bathymetry. Finally, the method is validated against experimental results for the run-up of a solitary wave on a sloped beach.

Keywords: Serre equations, dry bed

1. Introduction

Dispersion is an important phenomenon of waves in intermediate water depths; where the water depth is not much larger than the wavelengths of the waves. Our understanding of the effect of dispersion on water surface profiles is continually improving [1]. However, what is not well understood is the behaviour of these waves as they approach and then inundate the coastline.

There is a family of dispersive wave equations that can be used to model the behaviour of dispersive waves as they inundate a dry bed [2]. The Serre equations [3] are an important member of this family, as they do not make assumptions about the wave amplitude and so are fully non-linear. For this reason they are considered the most appropriate model of dispersive waves as they approach and then inundate the coastline [2].

There are many numerical methods for the Serre equations that are capable of modelling flows over dry beds [4–7]. The most popular approach for solving the Serre

*Corresponding author

Email addresses: jordan.pitt@anu.edu.au (J.P.A. Pitt), christopher.zoppou@anu.edu.au (C. Zoppou), stephen.roberts@anu.edu.au (S.G. Roberts)

equations is to split the Serre equations into their hyperbolic part given by the Shallow Water Wave Equations (SWWE) and their dispersive part [4, 6, 7]. Additionally, these splitting schemes employ modifications to simulate wave-breaking; where only the hyperbolic part is solved when some local wave breaking criteria is met.

Currently, there are no known analytic solutions to the Serre equations that include wetting and drying of a non-horizontal bed. Hence, numerical methods in the literature have relied on experimental results to demonstrate their capability in these situations [4–7]. We extend these validation results in the literature by using forced solutions of the Serre equations. Forced solutions allow the ability of the method to accurately solve problems containing the wetting and drying of bathymetry to be tested without analytic solutions. Furthermore, forced solutions permit a convergence analysis to demonstrate the order of accuracy of the method in these situations.

This paper also describes a new Finite Element Volume Method (FEVM) extension of the Finite Difference Volume Methods (FDVM) of Zoppou et al. [8]. In the FEVM a Finite Element Method (FEM) is used to solve the auxiliary elliptic equations instead of the finite difference methods used by the FDVM, leading to a more robust numerical method.

The Serre equations and their conservation properties are presented in the next section. Followed by a description of the FEVM. The numerical scheme will be validated against the lake at rest analytic solution, demonstrating that it is well-balanced. The method will then be validated for the wetting and drying of the bed using forced solutions to the Serre equations. Finally, the numerical method is validated against the experimental results of Synolakis [9] for the run-up of a solitary wave on a dry beach with a constant slope.

2. Serre Equations

The Serre equations [10] are a system of partial differential equations that describe the free-surface waves of fluids whose motion is dominated by gravitational forces. The primitive variables of the Serre equations are the height of the free-surface $h(x, t)$ above the bed $b(x)$ and the depth-averaged horizontal velocity of a column of water $u(x, t)$. These variables are shown in Figure 1. The absolute location of the free surface is given by $w(x, t) = h(x, t) + b(x)$.

The Serre equations can be written in conservation law form with a source term [8] like so

$$\frac{\partial h}{\partial t} + \frac{\partial(uh)}{\partial x} = 0, \quad (1a)$$

$$\begin{aligned} \frac{\partial G}{\partial t} + \frac{\partial}{\partial x} \left(uG + \frac{gh^2}{2} - \frac{2h^3}{3} \left[\frac{\partial u}{\partial x} \right]^2 + h^2 u \frac{\partial u}{\partial x} \frac{\partial b}{\partial x} \right) \\ + \underbrace{\frac{uh^2}{2} \frac{\partial u}{\partial x} \frac{\partial^2 b}{\partial x^2} - hu^2 \frac{\partial b}{\partial x} \frac{\partial^2 b}{\partial x^2} + gh \frac{\partial b}{\partial x}}_{\text{source term}} = 0 \end{aligned} \quad (1b)$$

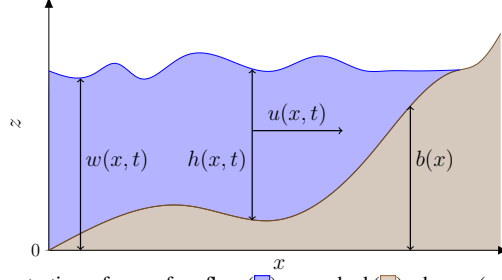


Figure 1: Diagram demonstrating a free surface flow (blue) over a bed (brown) where $w(x, t)$ is the absolute location of the free surface, $h(x, t)$ is the height of a column of fluid, $u(x, t)$ is the depth-averaged horizontal velocity of a column of fluid and $b(x)$ is the stationary bed profile.

46 with the conserved quantity

$$G = uh \left(1 + \frac{\partial h}{\partial x} \frac{\partial b}{\partial x} + \frac{h}{2} \frac{\partial^2 b}{\partial x^2} + \left[\frac{\partial b}{\partial x} \right]^2 \right) - \frac{\partial}{\partial x} \left(\frac{h^3}{3} \frac{\partial u}{\partial x} \right). \quad (2)$$

47 2.1. Conservation Properties

Since the Serre equations can be written in conservation law form with a source term for h and G these quantities should be conserved in a closed system, as long as the contribution of the source term is zero. Here conservation of a quantity q means that the total amount of q in a system occurring on the interval $[a, b]$ at time t

$$C_q(t) = \int_a^b q(x, t) dx$$

remains constant for all t . Additionally, the Serre equations conserve the momentum uh and the energy

$$\mathcal{H}(x, t) = \frac{1}{2} \left(gh(h + 2b) + hu^2 + \frac{h^3}{3} \left[\frac{\partial u}{\partial x} \right]^2 + u^2 h \left[\frac{\partial b}{\partial x} \right]^2 - uh^2 \frac{\partial u}{\partial x} \frac{\partial b}{\partial x} \right)$$

48 with \mathcal{H} being a sum of the gravitational potential and kinetic energy throughout the
 49 depth of water. The conservation of uh is a result of integrating the evolution of mo-
 50 mentum equation for the Serre equations [8]. An equivalent set of equations in one-
 51 dimension was derived by Green and Naghdi [11] through conservation of the energy
 52 \mathcal{H} , and hence the Serre equations also conserve \mathcal{H} .

53 3. Description of Numerical Method

54 To numerically approximate the Serre equations (1), the domain is partitioned into
 55 m cells $[x_{j-1/2}, x_{j+1/2}]$ of uniform length Δx . While time is discretised into time levels,
 56 t^n separated by a constant duration Δt .

Since the Serre equations are in conservation law form with a source term

$$\frac{\partial \mathbf{Q}}{\partial t} + \frac{\partial F(\mathbf{Q})}{\partial x} + S(\mathbf{Q}) = 0$$

57 with the conserved quantities $\mathbf{Q} = [h \ G]$, they can be solved using a Finite Volume
 58 Method (FVM) with a source term approximation like so

$$\bar{\mathbf{Q}}_j^{n+1} = \bar{\mathbf{Q}}_j^n - \frac{\Delta t}{\Delta x} (F_{j+1/2}^n(\bar{\mathbf{Q}}^n) - F_{j-1/2}^n(\bar{\mathbf{Q}}^n)) + \Delta t S_j^n(\bar{\mathbf{Q}}^n) \quad (3)$$

59 which employs first-order forward Euler time integration. The term $\bar{\mathbf{Q}}_j^n$ is the average of
 60 the conserved quantities in the j^{th} cell at time t^n . The approximations to the flux across
 61 the right and left boundaries of the cell are $F_{j+1/2}^n(\bar{\mathbf{Q}}^n)$ and $F_{j-1/2}^n(\bar{\mathbf{Q}}^n)$ respectively and
 62 $S_j^n(\bar{\mathbf{Q}}^n)$ is the approximation to the source terms contribution to the cell from time t^n to
 63 t^{n+1} . The FVM (3) produces a first-order time stepping method, second-order accuracy
 64 is achieved using a Strong Stability Preserving Runge-Kutta method [12] which uses a
 65 convex combination of (3).

66 To approximate the intercell fluxes $F_{j+1/2}^n(\bar{\mathbf{Q}}^n)$ and $F_{j-1/2}^n(\bar{\mathbf{Q}}^n)$ we use the method
 67 of Kurganov et al. [13]. The source term is approximated with the well-balancing
 68 modifications proposed by Audusse et al. [14].

69 To achieve a second-order accurate method using (3), second-order accurate ap-
 70 proximations to h , u , G , $\partial u/\partial x$, $\partial b/\partial x$, $\partial^2 b/\partial x^2$ inside a cell are required. The con-
 71 served quantities h and G are reconstructed from the cell averages, resulting in a linear
 72 approximation to h and G over the cell. The bed, b is reconstructed using a cubic poly-
 73 nomial to ensure that the approximation to $\partial^2 b/\partial x^2$ in the source term (1) is second-
 74 order accurate.

75 The depth-averaged velocity u is obtained by solving (2) with a FEM given the
 76 reconstructions of h , G and b over the cell. Thus all the required approximations are
 77 obtained allowing the use of (3) to solve (1) as desired.

78 3.1. Flux Approximation

79 The method of Kurganov et al. [13] was employed because it can handle disconti-
 80 nuities across the cell boundaries and only requires an estimate of the maximum and
 81 minimum wave speeds, which are known for the Serre equations [8].

82 Only the calculation of the flux term $F_{j+1/2}^n(\bar{\mathbf{Q}}^n)$ is demonstrated as the process to
 83 calculate the flux term $F_{j-1/2}^n(\bar{\mathbf{Q}}^n)$ is identical but involves different cells. For a general
 84 quantity q the approximation of the flux term given by Kurganov et al. [13] is

$$F_{j+1/2}^n(q) = \frac{a_{j+1/2}^+ f(q_{j+1/2}^-) - a_{j+1/2}^- f(q_{j+1/2}^+)}{a_{j+1/2}^+ - a_{j+1/2}^-} + \frac{a_{j+1/2}^+ a_{j+1/2}^-}{a_{j+1/2}^+ - a_{j+1/2}^-} (q_{j+1/2}^+ - q_{j+1/2}^-) \quad (4)$$

where $a_{j+1/2}^+$ and $a_{j+1/2}^-$ are given by bounds on the wave speed. With all the quantities
 on the right hand side representing their respective quantities at time t^n . Applying the
 wave speed bounds [8] we obtain

$$a_{j+1/2}^- = \min \left\{ 0, u_{j+1/2}^- - \sqrt{gh_{j+1/2}^-}, u_{j+1/2}^+ - \sqrt{gh_{j+1/2}^+} \right\}, \quad (5a)$$

$$a_{j+1/2}^+ = \max \left\{ 0, u_{j+1/2}^- + \sqrt{gh_{j+1/2}^-}, u_{j+1/2}^+ + \sqrt{gh_{j+1/2}^+} \right\}. \quad (5b)$$

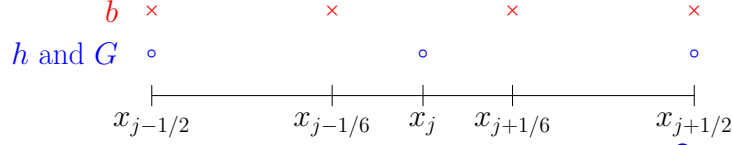


Figure 2: The conserved quantities h and G are reconstructed at $x_{j-1/2}$, x_j and $x_{j+1/2}$ (○) from their cell average values with a linear function over the cell. The bed, b is reconstructed at the equally spaced points $x_{j-1/2}$, $x_{j-1/6}$, $x_{j+1/6}$ and $x_{j+1/2}$ (×) from the nodal values with a cubic polynomial over the cell.

85

The flux functions $f(q_{j+1/2}^-)$ and $f(q_{j+1/2}^+)$ across the cell edge $x_{j+1/2}$ are evaluated using the reconstructed values $q_{j+1/2}^-$ from the j^{th} cell and $q_{j+1/2}^+$ from the $(j+1)^{\text{th}}$ cell. For the continuity equation (1a) we have

$$f(h_{j+1/2}^\pm) = u_{j+1/2}^\pm h_{j+1/2}^\pm \quad (6)$$

and for G , (1b) we obtain

$$\begin{aligned} f(G_{j+1/2}^\pm) &= u_{j+1/2}^\pm G_{j+1/2}^\pm + \frac{g}{2} (h_{j+1/2}^\pm)^2 - \frac{2}{3} (h_{j+1/2}^\pm)^3 \left[\left(\frac{\partial u}{\partial x} \right)_{j+1/2}^\pm \right]^2 \\ &\quad + (h_{j+1/2}^\pm)^2 u_{j+1/2}^\pm \left(\frac{\partial u}{\partial x} \right)_{j+1/2}^\pm \left(\frac{\partial b}{\partial x} \right)_{j+1/2}^\pm. \end{aligned} \quad (7)$$

86 The quantities $h_{j-1/2}^+$, $h_{j+1/2}^-$, $G_{j-1/2}^+$, $G_{j+1/2}^-$ and $(\partial b / \partial x)_{j+1/2}^\pm$ are given by the re-
87 constructions. While $u_{j+1/2}^\pm$ and $(\partial u / \partial x)_{j+1/2}^\pm$ are obtained by the FEM.

88 3.2. Reconstruction

89 We reconstruct h and G with piecewise linear functions over a cell from neighbour-
90 ing cell averages. While b is reconstructed from the nodal values of the neighbouring
91 cells $j-2$, $j-1$, $j+1$ and $j+2$ using a cubic polynomial over those cells. The cubic
92 polynomial ensures that the approximation to $\partial^2 b / \partial x^2$ in (1) is second-order accurate
93 in cell j . The location of the reconstructions for h , G and b are given in Figure 2, with
94 their corresponding reconstruction functions being the polynomials that pass through
95 their values at these locations. The bed is reconstructed at the cell edges and $x_{j\pm 1/6}$ as
96 these locations are equally spaced in the cell.

97 3.2.1. The conserved quantities, h and G

Since h and G use the same reconstruction operators we will demonstrate them for a general quantity q . The values of q are reconstructed at $x_{j-1/2}$, x_j and $x_{j+1/2}$ from the cell averages \bar{q}_j using the generalised minmod limiter [15]

$$q_{j-1/2}^+ = \bar{q}_j - \frac{\Delta x}{2} d_j, \quad q_j = \bar{q}_j, \quad q_{j+1/2}^- = \bar{q}_j + \frac{\Delta x}{2} d_j \quad (8)$$

98 where

$$d_j = \text{minmod} \left(\theta \frac{\bar{q}_j^n - \bar{q}_{j-1}^n}{\Delta x}, \frac{\bar{q}_{j+1}^n - \bar{q}_{j-1}^n}{2\Delta x}, \theta \frac{\bar{q}_{j+1}^n - \bar{q}_j^n}{\Delta x} \right) \quad (9)$$

99 with $\theta \in [1, 2]$. Note that although h and G have three reconstruction locations in Figure
 100 2, the resultant reconstructed function is a linear polynomial as the reconstructed nodal
 101 value is the average of the cell edge values.

102 3.2.2. Bed profile

The bed profile is reconstructed from the nodal values at the equally spaced locations $x_{j-1/2}$, $x_{j-1/6}$, $x_{j+1/6}$ and $x_{j+1/2}$ in the j^{th} cell demonstrated in Figure 2. To do this we use an interpolating cubic polynomial for b over the j^{th} cell

$$C_j(x) = c_0 (x - x_j)^3 + c_1 (x - x_j)^2 + c_2 (x - x_j) + c_3$$

that passes through the adjacent cell nodal values x_{j-2} , x_{j-1} , x_{j+1} and x_{j+2} and so has the coefficients

$$\begin{aligned} c_0 &= \frac{-b_{j-2} + 2b_{j-1} - 2b_{j+1} + b_{j+2}}{12\Delta x^3}, & c_1 &= \frac{b_{j-2} - b_{j-1} - b_{j+1} + b_{j+2}}{6\Delta x^2}, \\ c_2 &= \frac{b_{j-2} - 8b_{j-1} + 8b_{j+1} - b_{j+2}}{12\Delta x}, & c_3 &= \frac{-b_{j-2} + 4b_{j-1} + 4b_{j+1} - b_{j+2}}{6}. \end{aligned}$$

For the weak form of (2) to be valid, the bed profile must be continuous. To force a continuous bed profile the two possible values for b at the cell edges are averaged. Hence the reconstructions for b take the following values

$$b_{j\pm 1/2} = \frac{1}{2} (C_j(x_{j\pm 1/2}) + C_{j\pm 1}(x_{j\pm 1/2})), \quad b_{j\pm 1/6} = C_j(x_{j\pm 1/6}). \quad (10)$$

From these reconstruction values the reconstructed cubic polynomial for the bed profile

$$P_j^b(x) = p_0^b (x - x_j)^3 + p_1^b (x - x_j)^2 + p_2^b (x - x_j) + p_3^b$$

is the cubic polynomial that passes through the values (10) and therefore has the following coefficients

$$\begin{aligned} p_0^b &= \frac{-9b_{j-1/2} + 27b_{j-1/6} - 27b_{j+1/6} + 9b_{j+1/2}}{2\Delta x^3}, & p_1^b &= \frac{9b_{j-1/2} - 9b_{j-1/6} - 9b_{j+1/6} + 9b_{j+1/2}}{4\Delta x^2}, \\ p_2^b &= \frac{b_{j-1/2} - 27b_{j-1/6} + 27b_{j+1/6} - b_{j+1/2}}{8\Delta x}, & p_3^b &= \frac{-b_{j-1/2} + 9b_{j-1/6} + 9b_{j+1/6} - b_{j+1/2}}{16}. \end{aligned}$$

Therefore, the bed derivatives in (7) are approximated as follows

$$\left(\frac{\partial b}{\partial x} \right)_{j+1/2}^- = \frac{\partial}{\partial x} P_j^b(x_{j+1/2}), \quad \left(\frac{\partial b}{\partial x} \right)_{j+1/2}^+ = \frac{\partial}{\partial x} P_{j+1}^b(x_{j+1/2}). \quad (11)$$

103 *3.3. Calculating u and $\partial u/\partial x$*

To calculate u and $\partial u/\partial x$ a FEM is used to solve (2) for u given h , G and b . The FEM begins with the weak form of (2) using a test function v over the spatial domain Ω resulting in

$$\int_{\Omega} uh \left(1 + \frac{\partial h}{\partial x} \frac{\partial b}{\partial x} + \frac{1}{2} h \frac{\partial^2 b}{\partial x^2} + \left[\frac{\partial b}{\partial x} \right]^2 \right) v - \frac{\partial}{\partial x} \left(\frac{1}{3} h^3 \frac{\partial u}{\partial x} \right) v dx = \int_{\Omega} Gv dx.$$

Integrating by parts with zero Dirichlet boundary conditions gives

$$\begin{aligned} \int_{\Omega} uh \left(1 + \left[\frac{\partial b}{\partial x} \right]^2 \right) v dx + \int_{\Omega} \frac{1}{3} h^3 \frac{\partial u}{\partial x} \frac{\partial v}{\partial x} dx \\ - \int_{\Omega} \frac{1}{2} uh^2 \frac{\partial b}{\partial x} \frac{\partial v}{\partial x} dx - \int_{\Omega} \frac{1}{2} h^2 \frac{\partial b}{\partial x} \frac{\partial u}{\partial x} v dx = \int_{\Omega} Gv dx. \end{aligned} \quad (12)$$

104 Note that in the weak formulation we are able to remove a derivative on $h^3/3 (\partial u/\partial x)$
105 and reduce the double derivative of the bed to a single derivative.

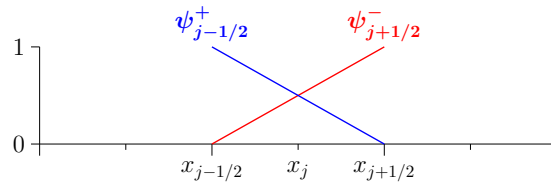
106 By assuming that time is fixed so that all the functions only vary in space, this
107 formulation implies that by ensuring that G , h , b and $\partial b/\partial x$ have finite integrals over
108 Ω , then u and $\partial u/\partial x$ must have finite integrals as well. To approximate the flux and the
109 source terms (1) requires $\partial u/\partial x$ to be well defined and thus have finite integrals. So we
110 will assume that for each time t that h and G are square integrable functions and b is in
111 the Sobolev space $\mathbb{H}^1(\Omega)$ where b and its first derivative are square integrable functions
112 so that u is also a member of $\mathbb{H}^1(\Omega)$.

To approximate (12) the integration is performed over the cells and then summed together to obtain the equation for the entire domain

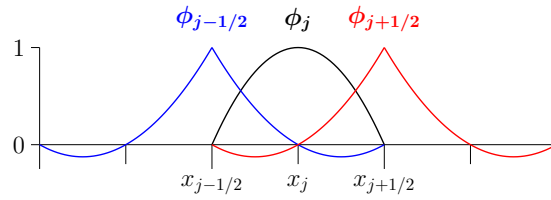
$$\begin{aligned} \sum_{j=1}^m \left(\int_{x_{j-1/2}}^{x_{j+1/2}} \left[\left(uh \left(1 + \left[\frac{\partial b}{\partial x} \right]^2 \right) - \frac{1}{2} h^2 \frac{\partial b}{\partial x} \frac{\partial u}{\partial x} \right) v \right. \right. \\ \left. \left. + \left(\frac{1}{3} h^3 \frac{\partial u}{\partial x} - \frac{1}{2} uh^2 \frac{\partial b}{\partial x} \right) \frac{\partial v}{\partial x} \right] dx \right) = \sum_{j=1}^m \left(\int_{x_{j-1/2}}^{x_{j+1/2}} Gv dx \right) \end{aligned} \quad (13)$$

113 which holds for all test functions v . The next step is to replace the functions for h , G ,
114 b , v and u with their corresponding basis function approximations.

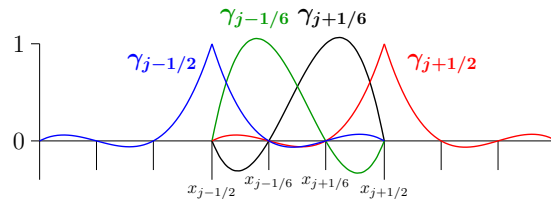
115 For h and G the basis functions ψ are linear inside a cell and zero elsewhere, re-
116 sulting in approximations that are square integrable, as desired. For u and v the basis
117 functions ϕ which are quadratic inside the cell and continuous across the cell edges are
118 used so that the approximations are in $\mathbb{H}^1(\Omega)$. The basis functions of u are quadratics
119 to allow for a second-order approximation to $\partial u/\partial x$ in (7). Finally, for b the basis func-
120 tions γ are used, they are cubic polynomials inside the cell and continuous across the
121 cell edges so that the approximation to b is in the appropriate function space. Cubic
122 polynomials are used for b as a second-order approximation to $\partial^2 b/\partial x^2$ is required for
123 the source term in (1). Examples of the basis functions ψ , ϕ and γ for the j^{th} cell are
124 given in Figure 3, from which their equations can be derived.



(a) ψ



(b) ϕ



(c) γ

Figure 3: Support of the basis functions ψ , ϕ and γ which are non-zero over the j^{th} cell.

125 The basis function approximation to h and G in the FEM written for a generic
 126 quantity q is

$$q = \sum_{j=1}^m (q_{j-1/2}^+ \psi_{j-1/2}^+ + q_{j+1/2}^- \psi_{j+1/2}^-) \quad (14a)$$

127 while for u it is

$$u = u_{1/2} \phi_{1/2} + \sum_{j=1}^m (u_j \phi_j + u_{j+1/2} \phi_{j+1/2}) \quad (14b)$$

128 and finally for b it is

$$b = b_{1/2} \gamma_{1/2} + \sum_{j=1}^m (b_{j-1/6} \gamma_{j-1/6} + b_{j+1/6} \gamma_{j+1/6} + b_{j+1/2} \gamma_{j+1/2}). \quad (14c)$$

129 Substituting all the functions in (13) with their corresponding basis function approxi-
 130 mations (14) the integral equation becomes a matrix equation. Assembling these ma-
 131 trices results in

$$\mathbf{A} \hat{\mathbf{u}} = \mathbf{g}. \quad (15)$$

132 Where \mathbf{A} is the stiffness matrix given by the integrals that contain u , $\hat{\mathbf{u}}$ is the vector
 133 containing the cell edge and nodal values of u and \mathbf{g} is given by the integral of Gv .
 134 This is a penta-diagonal matrix equation which can be solved by direct banded matrix
 135 solution techniques such as those of Press et al. [16] to obtain $\hat{\mathbf{u}}$ and thus $u_{j+1/2}^\pm$ as
 136 desired. Note that $u_{j+1/2}^\pm = u_{j+1/2}$ since u is continuous at the cell edges.

To calculate $(\partial u / \partial x)_{j+1/2}^\pm$ we take the derivative of (14b). Since only $\phi_{j-1/2}$, ϕ_j and
 $\phi_{j+1/2}$ are non-zero over the j^{th} cell we have that

$$\left(\frac{\partial u}{\partial x} \right)_{j+1/2}^- = u_{j-1/2} \frac{\partial \phi_{j-1/2}}{\partial x} + u_j \frac{\partial \phi_j}{\partial x} + u_{j+1/2} \frac{\partial \phi_{j+1/2}}{\partial x}, \quad (16a)$$

$$\left(\frac{\partial u}{\partial x} \right)_{j+1/2}^+ = u_{j+1/2} \frac{\partial \phi_{j+1/2}}{\partial x} + u_{j+1} \frac{\partial \phi_{j+1}}{\partial x} + u_{j+3/2} \frac{\partial \phi_{j+3/2}}{\partial x} \quad (16b)$$

137 where the derivatives of the basis functions ϕ are evaluated at $x_{j+1/2}$.

138 3.4. Source Term Approximation

139 To evolve the Serre equations using (3) requires an approximation to $S_j^n(\bar{\mathcal{Q}}^n)$. Equa-
 140 tion (1a) has no source term, therefore only the calculation of the source term for equa-
 141 tion (1b) is presented.

142 Since (3) is first-order accurate in time the source term approximation

$$S_j^n(\bar{\mathcal{Q}}^n) = -\frac{1}{2} (h_j^n)^2 u_j^n \left(\frac{\partial u}{\partial x} \right)_j^n \left(\frac{\partial^2 b}{\partial x^2} \right)_j^n + h_j^n (u_j^n)^2 \left(\frac{\partial b}{\partial x} \right)_j^n \left(\frac{\partial^2 b}{\partial x^2} \right)_j^n - g h_j^n \left(\frac{\partial b}{\partial x} \right)_j^n \quad (17)$$

is sufficient. The quantities h_j^n and u_j^n are given by (8) and (15) respectively. To calcu-
 late the derivatives of b and u the approximations outlined in (11) and (14b) respectively
 are used to obtain

$$\left(\frac{\partial b}{\partial x} \right)_j = \frac{\partial}{\partial x} P_j^b(x_j), \quad \left(\frac{\partial^2 b}{\partial x^2} \right)_j = \frac{\partial^2}{\partial x^2} P_j^b(x_j),$$

$$\left(\frac{\partial u}{\partial x}\right)_j = u_{j-1/2} \frac{\partial \phi_{j-1/2}}{\partial x} + u_j \frac{\partial \phi_j}{\partial x} + u_{j+1/2} \frac{\partial \phi_{j+1/2}}{\partial x}$$

where the derivatives of the ϕ basis functions are evaluated at x_j . We therefore have all the required approximations to perform the FVM (3) and obtain a temporally first-order approximation to (1).

3.5. Courant-Frederichs-Lewy Condition

To ensure the stability of the FVM (3) the Courant-Friedrichs-Lewy (CFL) condition [17] is used. The CFL condition is necessary for stability and ensures that time steps are small enough so that information is only transferred between neighbouring cells. For the Serre equations the CFL condition is

$$\Delta t \leq \frac{Cr}{\max_j \{a_{j+1/2}^\pm\}} \Delta x \quad (19)$$

where $a_{j+1/2}^\pm$ are the wave-speed bounds used in the flux approximation (5) and $0 \leq Cr \leq 1$ is the Courant number. Typically, we use the conservative $Cr = 0.5$ for our numerical experiments.

3.6. Time-Stepping

To increase the order of accuracy in time we employ the second-order SSP Runge-Kutta method [12] which is a convex combination of first-order forward Euler time steps (3) in the following way

$$\bar{\mathcal{Q}}_j^{(1)} = \bar{\mathcal{Q}}_j^n - \frac{\Delta t}{\Delta x} (F_{j+1/2}^n(\bar{\mathcal{Q}}_j^n) - F_{j-1/2}^n(\bar{\mathcal{Q}}_j^n)) + \Delta t S_j^n(\bar{\mathcal{Q}}_j^n), \quad (20a)$$

$$\bar{\mathcal{Q}}_j^{(2)} = \bar{\mathcal{Q}}_j^{(1)} - \frac{\Delta t}{\Delta x} (F_{j+1/2}^{(1)}(\bar{\mathcal{Q}}_j^{(1)}) - F_{j-1/2}^{(1)}(\bar{\mathcal{Q}}_j^{(1)})) + \Delta t S_j^{(1)}(\bar{\mathcal{Q}}_j^{(1)}), \quad (20b)$$

$$\bar{\mathcal{Q}}_j^{n+1} = \frac{1}{2} (\bar{\mathcal{Q}}_j^n + \bar{\mathcal{Q}}_j^{(2)}) \quad (20c)$$

This results in a time stepping method that preserves the stability of the first-order method and is second-order accurate in time. Since all the spatial approximations are second-order accurate, the FEVM should be a second-order accurate solver for the Serre equations.

3.7. Well Balancing Modifications

To ensure that the method is well-balanced the work of Audusse et al. [14] is followed. This method was originally designed for the SWWE but was shown to apply equally well to the Serre equations [18].

The well balancing approach makes two changes to the method outlined above. The well-balancing introduces a different reconstruction of h that is used in the flux terms (6) and (7). Additionally, correction terms are added to the source term approximation (17). These changes ensure that the numerical approximations to the hydrostatic pressure term in the flux and the source term cancel for the lake at rest problem, where a still lake has a horizontal water surface.

169 *3.7.1. Modified Reconstruction of h*

The modified reconstruction of h , \bar{h} depends on the reconstructions $w_{j+1/2}^\pm$ of w at the cell edge, which is calculated from its cell average values in the same way as h and G , (9). From these reconstructions the bed values

$$\tilde{b}_{j+1/2}^- = w_{j+1/2}^- - h_{j+1/2}^-, \quad \tilde{b}_{j+1/2}^+ = w_{j+1/2}^+ - h_{j+1/2}^+$$

are calculated. Since $\tilde{b}_{j+1/2}^\pm$ are calculated from two reconstructions that are discontinuous across the cell edges they are also discontinuous across the cell edges, unlike the reconstruction of the bed profile in (10). Given the maximum of these reconstructed bed values

$$\bar{\bar{b}}_{j+1/2} = \max\{\tilde{b}_{j+1/2}^-, \tilde{b}_{j+1/2}^+\}$$

the reconstruction \bar{h} at the cell edges is given by

$$\bar{\bar{h}}_{j+1/2}^- = \max\{0, w_{j+1/2}^- - \bar{\bar{b}}_{j+1/2}\}, \quad \bar{\bar{h}}_{j+1/2}^+ = \max\{0, w_{j+1/2}^+ - \bar{\bar{b}}_{j+1/2}\} \quad (21)$$

170 which replaces $h_{j+1/2}^\pm$ in the flux terms (6) and (7).

171 *3.7.2. Modified Source Term*

The source term is modified by adding the corrective interface source terms $S_{j+1/2}^-(\bar{\mathcal{Q}}_j^n)$ and $S_{j-1/2}^+(\bar{\mathcal{Q}}_j^n)$ to obtain

$$S_j^n(\bar{\mathcal{Q}}_j^n) = \frac{1}{\Delta x} S_{j+1/2}^-(\bar{\mathcal{Q}}_j^n) + S_{ci}(\bar{\mathcal{Q}}_j^n) + \frac{1}{\Delta x} S_{j-1/2}^+(\bar{\mathcal{Q}}_j^n).$$

The term $S_{ci}(\bar{\mathcal{Q}}_j^n)$ is the source term approximation given in (17) with the approximation to $\partial b / \partial x$ altered to depend on $\tilde{b}_{j+1/2}^\pm$ like so

$$\left(\frac{\partial b}{\partial x}\right)_j = \frac{\tilde{b}_{j+1/2}^- - \tilde{b}_{j-1/2}^+}{\Delta x}.$$

The corrective interface source terms are calculated in the following way

$$S_{j+1/2}^-(\bar{\mathcal{Q}}_j^n) = \frac{g}{2} (\bar{\bar{h}}_{j+1/2}^-)^2 - \frac{g}{2} (h_{j+1/2}^-)^2, \quad S_{j-1/2}^+(\bar{\mathcal{Q}}_j^n) = \frac{g}{2} (h_{j-1/2}^+)^2 - \frac{g}{2} (\bar{\bar{h}}_{j-1/2}^+)^2.$$

172 These corrective terms ensure that when $u = 0$ and the water surface is horizontal, that
 173 $S_j^n = (F_{j+1/2}^n - F_{j-1/2}^n) / \Delta x$, keeping the method well-balanced. The correction terms
 174 make use of $h_{j+1/2}^\pm$ obtained from the reconstruction (8) and the other reconstructions
 175 $\bar{\bar{h}}_{j+1/2}^\pm$ from (21).

176 *3.8. Dry Bed Handling Modifications*

177 Dry beds present two issues for the FEM; (i) when h and G are small then small
 178 errors in h and G can produce large errors in u leading to instabilities and (ii) when
 179 $h = 0$ the stiffness matrix \mathbf{A} , (15) becomes singular.

Issue (i), where large errors in u are produced when h is small also arises when solving the SWWE; due to $u = (uh)/h$ being undefined as uh and h vanish. For the Serre equations with horizontal beds, from (2) when $h \ll 1$ we have

$$G = uh + O(h^3).$$

Since $h \ll 1$ the $O(h^3)$ terms can be neglected, and thus when h is small G is approximately equal to the momentum uh . Hence, the challenges posed by $h \rightarrow 0$ for the SWWE and the Serre equations are similar. Therefore, dry bed handling techniques from the SWWE such as the desingularisation transformations of Kurganov and Petrova [19] can be applied to the Serre equations.

These desingularisation transforms act by modifying the calculation of u given h and uh to avoid the singularity as the numerator and denominator approach zero, hence their name. The simplest such transformation is

$$u = \frac{(uh)h}{h^2 + \epsilon} \quad (22)$$

where ϵ is some small chosen parameter. The error introduced by this transformation is smallest when ϵ is smallest. However, as noted by Kurganov and Petrova [19] small values of ϵ lead to large numerical errors in the calculation of u . To avoid such errors ϵ can be made larger or following Kurganov and Petrova [19] a different desingularisation transformation can be employed. For the validations described later, we found the simpler transformation with small values of ϵ more useful, keeping in mind that large numerical errors in u were possible for small values of h .

To adapt the calculation of u in (22) to (2) we view it as a transformation of the quantity h which is equivalent to

$$h \rightarrow \frac{h^2 + \epsilon}{h}. \quad (23)$$

Therefore, our transformation for the reconstructed values of h in the FEM is

$$h_{j-1/2}^\pm = \frac{(h_{j-1/2}^\pm)^2 + \epsilon}{h_{j-1/2}^\pm} \quad (24)$$

where on the right hand side are the reconstructed values of h from (8) and the left hand side are the values of h used to defined the basis functions of the FEM (14a). In the numerical experiments in this paper, we set $\epsilon = 10^{-8}$. The transformation (24) is applied to all terms containing h in the FEM avoiding the singularity as $h \rightarrow 0$.

To resolve issue (ii), \mathbf{A} becoming singular when h vanishes we only solve (15) for u in wet cells. Wet and dry cells are identified using the cell average \bar{h} ; a cell is considered dry when $\bar{h}_j \leq h_{tol}$ and wet otherwise. For dry cells we set

$$\begin{aligned} h_{j-1/2}^+ &= 0, & G_{j-1/2}^+ &= 0, & w_{j-1/2}^+ &= b_{j-1/2}, \\ h_j &= 0, & G_j &= 0, & w_j &= b_j, \\ h_{j+1/2}^- &= 0, & G_{j+1/2}^- &= 0, & w_{j+1/2}^- &= b_{j+1/2}, \\ u_j &= 0 \end{aligned}$$

and if the neighbouring cells are dry then the velocity at the cell edges vanish so that

$$\begin{aligned} u_{j-1/2} &= 0 & \text{when } \bar{h}_{j-1} \leq h_{tol}, \\ u_{j+1/2} &= 0 & \text{when } \bar{h}_{j+1} \leq h_{tol}. \end{aligned}$$

For the numerical experiments in this paper we used $h_{tol} = 10^{-12}$.

To ensure that the matrix solve of (15) is robust in the presence of small values of h , we employ an LU decomposition with partial pivoting [16]. Typically, we set the pivot tolerance value $p_{tol} = 10^{-20}$.

4. Validation

To validate that the numerical method has the appropriate order of accuracy, well-balanced and can handle dry-beds we will use an analytic solution, forced solution and experimental results. Firstly, the convergence and conservation properties of the method for the lake at rest analytic solution are established. Secondly, we demonstrate the convergence of the numerical method to a forced solution of the Serre equations. Finally, we compare our numerical solutions to the experimental results of Synolakis [9].

4.1. Measures of Error

We begin the validation by defining the measures of error and conservation error for a general quantity q . The L_2 vector norm was used to measure the error between a numerical solution at the cell nodes \mathbf{q}^* and the analytic or forced solution at the cell nodes \mathbf{q} using

$$L_2(\mathbf{q}, \mathbf{q}^*) = \begin{cases} \frac{\|\mathbf{q}^* - \mathbf{q}\|_2}{\|\mathbf{q}\|_2} & \|\mathbf{q}\|_2 > 0 \\ \|\mathbf{q}^*\|_2 & \|\mathbf{q}\|_2 = 0. \end{cases}$$

By investigating the behaviour of $L_2(\mathbf{q}, \mathbf{q}^*)$ for numerical solutions with various Δx values we can establish the convergence rate of the method.

The conservation properties of the method are studied using the conservation error

$$C^*(\mathbf{q}, \mathbf{q}^*) = \begin{cases} \frac{|C^*(\mathbf{q}^*) - C^*(\mathbf{q})|}{|C^*(\mathbf{q})|} & |C^*(\mathbf{q})| > 0 \\ |C^*(\mathbf{q}^*)| & |C^*(\mathbf{q})| = 0. \end{cases}$$

The conservation error $C^*(\mathbf{q}, \mathbf{q}^*)$ compares the total amount of q in the numerical solution at the end of the simulation $C^*(\mathbf{q}^*)$ to the total amount of q in the initial conditions $C^*(\mathbf{q})$. The total amount of a quantity is calculated numerically by summing the total amount of q in each cell. Fifth-order accurate Gaussian quadrature of a quartic interpolation of q , using the neighbouring nodal values is used to calculate the total amount of q in a cell.

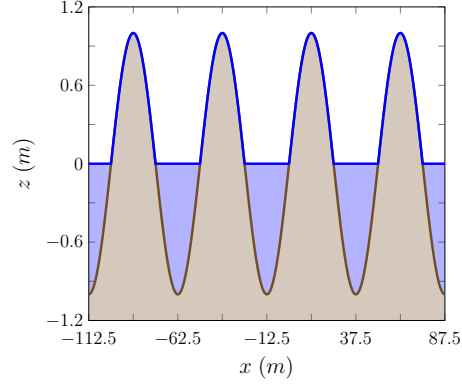


Figure 4: Numerical solution for w (blue) and b (brown) with $\Delta x = 100/2^{10}m$ for the lake at rest problem at $t = 10s$.

223 4.2. Lake at Rest Solution Validation

224 The lake at rest is a stationary analytic solution of the Serre equations where a still
 225 lake has a horizontal water surface over any bathymetry. This solution is maintained
 226 due to the balance of the hydrostatic pressure and the forcing of the bed slope. A well-
 227 balanced numerical method should accurately reproduce this lake at rest stationary
 228 solution.

To test whether this method is well-balanced we chose the following lake at rest solution

$$\begin{aligned} h(x, t) &= \max \{a_0 - b(x), 0\}, & b(x) &= a_1 \sin(a_2 x), \\ u(x, t) &= 0, & G(x, t) &= 0. \end{aligned}$$

229 To demonstrate the capability of the method in the presence of dry and wet regions of
 230 the bed, the parameter values $a_0 = 0m$, $a_1 = 1m$ and $a_2 = 2\pi/50m^{-1}$ were chosen.
 231 These parameter values result in lakes with a horizontal free surface surrounded by dry
 232 regions.

233 For the numerical solutions the spatial domain was $x \in [-112.5m, 87.5m]$ and the
 234 final time was $t = 10s$, with the standard gravitational acceleration $g = 9.81m/s^2$. The
 235 spatial resolution of the method was varied so that $\Delta x = 100/2^k m$ with $k \in [8, \dots, 17]$
 236 and the CFL condition (19) was satisfied by having $\Delta t = Cr\Delta x / \sqrt{g}$ with condition
 237 number $Cr = 0.5$. The generalised limiter parameter $\theta = 1.2$ was used in (9). Dirichlet
 238 boundary conditions were used at both ends as the analytic solution is stationary.

239 The numerical method is assessed by comparing the numerical solution at $t = 10s$
 240 to the analytic solution, which are the initial conditions.

241 An example numerical solution with $\Delta x = 100/2^{10}m \approx 0.0977m$ at $t = 10s$ is given
 242 in Figure 4. The numerical solution in this Figure is indistinguishable from the analytic
 243 solution at this scale and so the analytic solution has been omitted.

244 Examination of the L_2 errors depicted in Figure 5(a) reveals that the method repro-
 245 duced h , G and u precisely, accounting for round-off errors. The errors for h , G and u
 246 are increasing as $\Delta x \rightarrow 0$ due to an accumulation of the round-off errors.

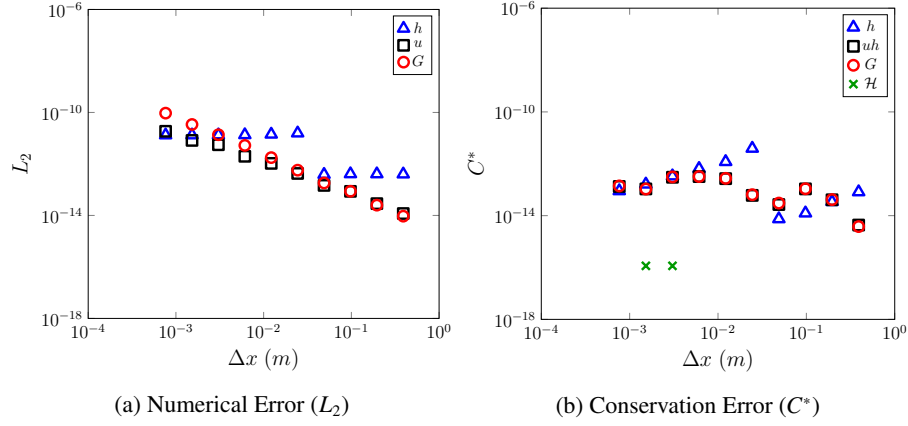


Figure 5: The numerical error (h , u and G) and conservation error (h , uh , G and \mathcal{H}) against Δx for the lake at rest problem at $t = 10s$.

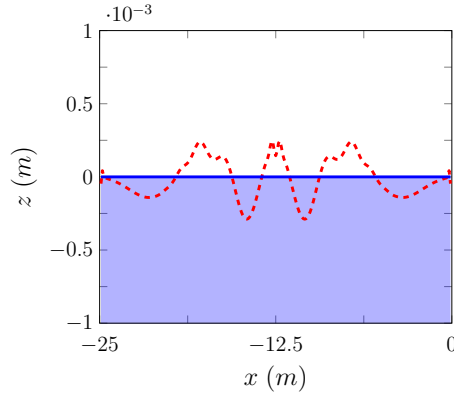


Figure 6: Numerical solution for w with (—) and without (---) well-balancing modifications over $[-25, 0]$ for the lake at rest problem at $t = 10s$ where $\Delta x = 100/2^{10}m$.

247 The conservation errors as measured by C^* for h , uh , G and \mathcal{H} are given in Figure
 248 5(b). The conservation error of these conserved quantities demonstrates that all quanti-
 249 ties are conserved within machine precision, with \mathcal{H} being conserved exactly for most
 250 numerical solutions, hence its disappearance from the log-log plot. The conservation
 251 error of \mathcal{H} is small for the lake at rest solution since u and therefore the kinetic energy
 252 vanish.

253 These results demonstrate that the developed method has accurately reproduced
 254 the lake at rest solution and is therefore well-balanced. Without the employed well-
 255 balancing modifications the numerical solution quickly develops non-zero velocities
 256 and a non-horizontal water surface profile as can be seen in Figure 6.

257 *4.3. Forced Solution Validation*

258 There are currently no known analytic solution of the Serre equations for the wet-
 259 ting and drying of bathymetry. To test the capability of our numerical method in this
 260 environment we resort to a forced solution.

To generate a forced solution we select some arbitrary functions for all of the prim-
 itive quantities; h , u and b which we denote by $h^\#$, $u^\#$ and $b^\#$ respectively. To ensure
 that these functions $h^\#$, $u^\#$ and $b^\#$ are exact solutions the Serre equations are modified
 by adding the terms S_h and S_G to obtain the forced Serre equations

$$\begin{aligned} \frac{\partial h}{\partial t} + \frac{\partial(uh)}{\partial x} + S_h &= 0, \\ \frac{\partial G}{\partial t} + \frac{\partial}{\partial x} \left(uG + \frac{gh^2}{2} - \frac{2h^3}{3} \left[\frac{\partial u}{\partial x} \right]^2 + h^2 u \frac{\partial u}{\partial x} \frac{\partial b}{\partial x} \right) \\ &+ \frac{uh^2}{2} \frac{\partial u}{\partial x} \frac{\partial^2 b}{\partial x^2} - hu^2 \frac{\partial b}{\partial x} \frac{\partial^2 b}{\partial x^2} + gh \frac{\partial b}{\partial x} + S_G = 0 \end{aligned}$$

where

$$\begin{aligned} S_h &= -\frac{\partial h^\#}{\partial t} - \frac{\partial(u^\# h^\#)}{\partial x}, \\ S_G &= -\frac{\partial G^\#}{\partial t} - \frac{\partial}{\partial x} \left(u^\# G^\# + \frac{g[h^\#]^2}{2} - \frac{2[h^\#]^3}{3} \left[\frac{\partial u^\#}{\partial x} \right]^2 + [h^\#]^2 u^\# \frac{\partial u^\#}{\partial x} \frac{\partial b^\#}{\partial x} \right) \\ &\quad - \frac{u^\# [h^\#]^2}{2} \frac{\partial u^\#}{\partial x} \frac{\partial^2 b^\#}{\partial x^2} + h^\# [u^\#]^2 \frac{\partial b^\#}{\partial x} \frac{\partial^2 b^\#}{\partial x^2} - gh^\# \frac{\partial b^\#}{\partial x}. \end{aligned}$$

261 These forced Serre equations are then numerically solved by solving the Serre equa-
 262 tions (1) with the analytic values of S_h and S_G given $h^\#$, $u^\#$ and $b^\#$. Hence, the only
 263 error present in the numerical solutions of the forced Serre equations is the error pro-
 264 duced by the numerical method used to solve the original Serre equations.

265 Note that since the choice of the forced solutions $h^\#$, $u^\#$ and $b^\#$ is arbitrary the
 266 solutions of the forced Serre equations need not be conservative or retain any properties
 267 of the underlying Serre equations.

268 4.3.1. Dry Bed Forced Solution Problem

To test the capability of the numerical method to solve the Serre equations the following expressions were chosen

$$h^\#(x, t) = a_0 \exp\left(-\frac{[(x - a_1 t) - a_2]^2}{2a_3}\right), \quad (25a)$$

$$u^\#(x, t) = a_4 \exp\left(-\frac{[(x - a_1 t) - a_2]^2}{2a_3}\right), \quad (25b)$$

$$b^\#(x) = a_5 \sin(a_6 x) \quad (25c)$$

269 for the primitive variables. These functions produce a Gaussian bump for h and u that
 270 travels at a fixed speed a_1 over a dry periodic bed. Thus, h and u will have constant
 271 shape and travel in the positive x direction over time. The quantity G will not maintain
 272 a constant shape due to its dependence on the bed slope which varies over x .

273 The values $a_0 = 0.5m$, $a_1 = 2\pi/(10a_7)m/s$, $a_2 = -3\pi/(2a_6)m$, $a_3 = \pi/(16a_6)m^2$,
 274 $a_4 = 0.5m/s$, $a_5 = 1.0m$ and $a_6 = \pi/25m^{-1}$ were used. These parameter values produce
 275 a Gaussian bump in h and u that has a width much smaller than the wavelength of the
 276 bed profile and travels precisely one wavelength of the bed in 10s.

277 The domain of the numerical solutions was $x \in [-112.5m, 87.5m]$ with $t \in [0s, 10s]$.
 278 The standard gravitational acceleration $g = 9.81m/s^2$ was used. The spatial resolution
 279 of numerical methods was varied like so $\Delta x = 100/2^k m$ with $k \in [8, \dots, 17]$. To satisfy
 280 the CFL condition (19) the temporal resolution $\Delta t = Cr\Delta x/(a_1 + a_4 + \sqrt{g(a_0)})$ was
 281 chosen with condition number $Cr = 0.5$. The value $\theta = 1.2$ was used in the generalised
 282 minmod limiter (9) and Dirichlet boundary conditions were applied at the boundaries
 283 of the domain.

284 Plots of w , h , u and G are given in Figure 7 for the numerical solution with $\Delta x =$
 285 $100/2^{12}m \approx 0.0024m$. The numerical solutions of w , h and G well reproduce their
 286 respective forced solutions. However, u contains significant errors behind the Gaussian
 287 bump, these errors depend on $\epsilon = 10^{-8}$, $h_{tol} = 10^{-12}$ and Δx . For larger values of ϵ and
 288 h_{tol} the errors in u can be significantly damped [19]. However, if ϵ and h_{tol} are larger
 289 they begin to dominate the L_2 errors for larger Δx values making the convergence rate of
 290 the method less obvious. This trade-off is present for all desingularisation transforms.

291 By varying the Δx values the errors in u decrease, which can be observed in the L_2
 292 errors in Figure 8. For h and G the desired second-order accuracy is achieved for the
 293 entire range of Δx values. The velocity, u also attains second-order accuracy for Δx
 294 values around 10^{-2} however, the second-order accuracy is lost as Δx decreases further.
 295 This plateau in the error for small Δx values is due to the desingularisation techniques
 296 error in approximating h with (24) using $\epsilon = 10^{-8}$. When $h \approx 10^{-4}$ then $h^2 \approx \epsilon$ and the
 297 errors introduced by (24) become significant, hindering further reduction in the error
 298 of the velocity below 10^{-4} . To circumvent this requires lowering ϵ further which can
 299 significantly increase the error in the velocity [19]. Importantly, these errors in u are
 300 not transmitted to h and G as they occur when h is small and all the flux and source
 301 terms that include u are multiplied by some power of h .

302 The goal of using this forced solution was to confirm the convergence rate of the
 303 numerical method for the wetting and drying of variables beds. For this purpose the

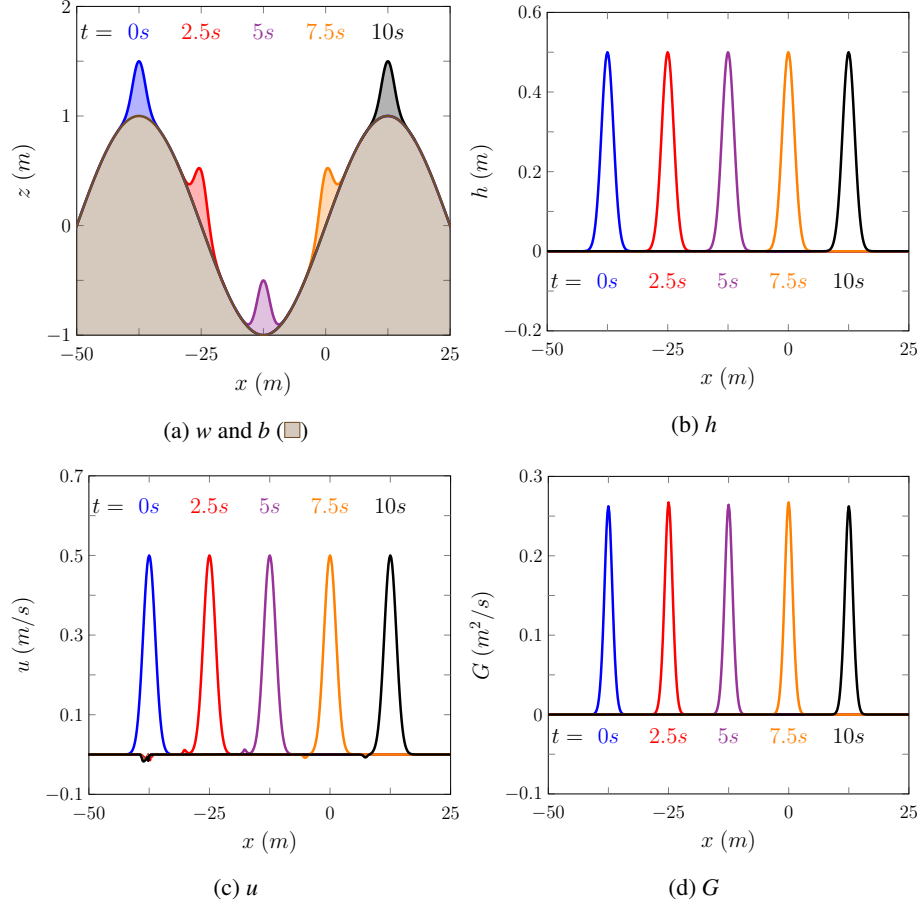
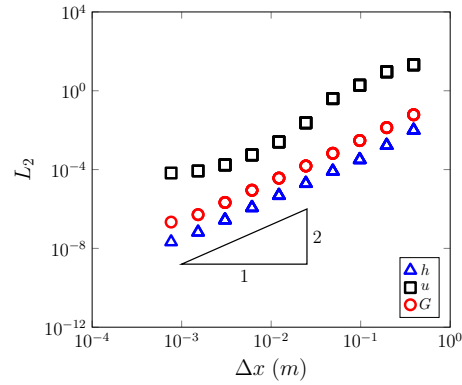


Figure 7: Example numerical solutions for w , b , h , G with $\Delta x = 100/2^{12}m$ at various times to the dry bed forced solution problem.



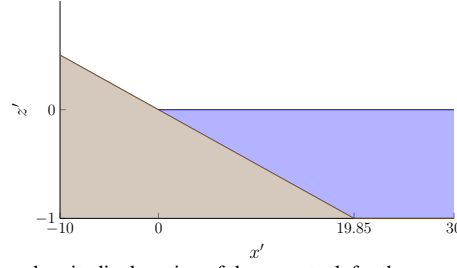


Figure 9: Diagram showing a longitudinal section of the wave tank for the run-up experiment with the water (blue) and the bed (brown) where the coordinates have been non-dimensionalised [9].

chosen desingularisation transform (24) with these ϵ and h_{tol} values was sufficient. These results demonstrate that described FEVM reproduced the forced solution well, validating the method for flows over dry bathymetry.

4.4. Run-up of a Solitary Wave

To study the run-up of incoming waves on linear beaches a series of experiments were conducted by Synolakis [9]. These experiments consisted of a number of run-up events for a wide array of breaking and non-breaking waves where snapshots of the entire water surface were taken at certain times. These experiments were all performed on the beach profile depicted in Figure 9, where all the quantities are non-dimensionalised [9]. To denote that a quantity is non-dimensionalised we use a prime. To assess the numerical method we recreated one of these experiments, which captured the run-up of a non-breaking solitary wave.

The numerical method used the non-dimensionalised quantities reported by Synolakis [9] to reproduce the experiment. The spatial domain was $x' \in [-30, 150]$ with a resolution of $\Delta x = 0.05$ and was run until $t' = 250$ with the CFL condition (19) satisfied by setting $\Delta t = 0.1\Delta x$. The spatial reconstruction used $\theta = 1.2$ and the acceleration due to gravity $g = 1$ was chosen to match the non-dimensionalisation.

The same initial conditions are used to construct this numerical experiment as those of Li et al. [5], producing the initial water surface profile depicted in Figure 9.

The non-dimensionalised water surface data is given at the various times in Figure 11. The error in conservation of h' , $u'h'$, G' and \mathcal{H}' by $t' = 250$ as measured by C^* are given in Table 1.

The numerical solution reproduces the incoming wave properties and the maximum run-up well, and compares well to numerical solutions presented in the literature [5, 6]. The experimental wave appears to be more skewed towards the shoreline, but this shape difference has all but disappeared as the wave begins to inundate the shore. The only other noticeable difference is that the numerical solution appears to recede further than the experimental results. The observed larger run-down is likely caused by the omission of bed friction for the Serre equations in this paper.

Both h' and \mathcal{H}' are well conserved by the method throughout the run-up and run-down of the wave, particularly h' . The total energy \mathcal{H}' of the method is also well conserved, however \mathcal{H}' appears to have slightly increased in the method during the run-up process due to the methods handling of the dry bed problem. During this experiment

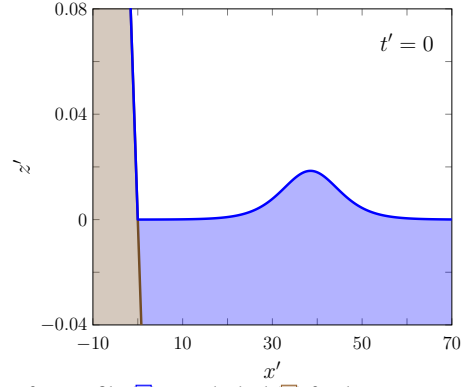


Figure 10: Initial water surface profile (blue line) over the bed (brown shaded area) for the run-up experiment of Synolakis [9].

Quantity	$C^*(q^0)$	$C^*(q^*)$	$C^*(q^0, q^*)$
h'	2.40×10^2	2.40×10^2	1.33×10^{-10}
$u'h'$	-3.19×10^{-2}	3.19×10^{-2}	4.96×10^{-4}
G'	-3.19×10^{-2}	3.19×10^{-2}	5.88×10^{-4}
\mathcal{H}'	-1.18×10^2	-1.18×10^2	3.77×10^{-7}

Table 1: Initial and final ($t' = 250$) total amounts and the conservation error for the conserved quantities in the numerical solution of the run-up experiment. Here the absolute value of the total amount of uh and G are taken in the error as the wave has reflected off the beach.

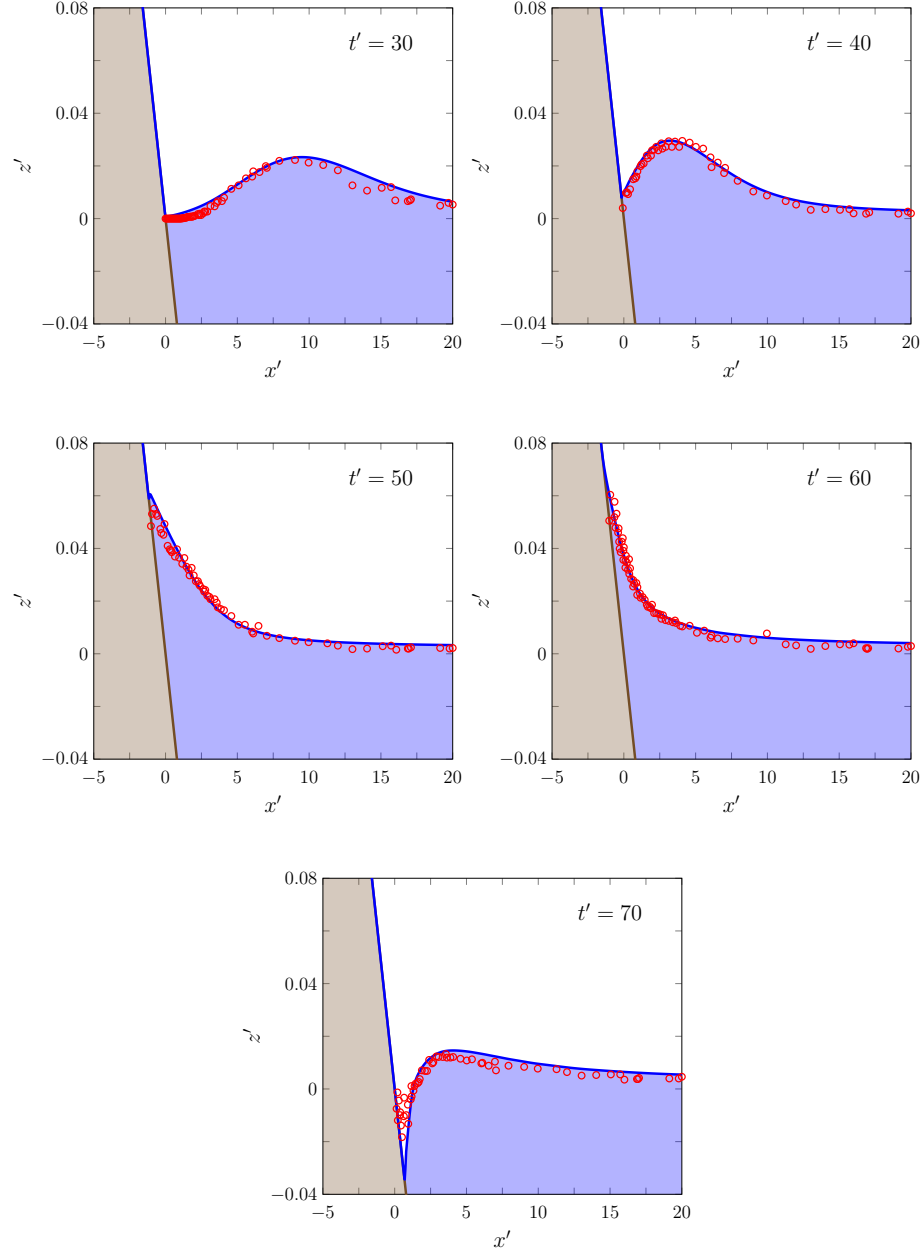


Figure 11: A comparison of the water surface profiles $w'(x', t')$ for the experiment (○) and the numerical solution (—) over the bed (■) at various times.

kinetic energy is converted into gravitational potential energy and then back again as the wave is reflected. By $t' = 250$ the reflection of the wave is complete and so we can see that the total amount of $u'h'$ and G' have changed signs, although their errors are small if this is considered. Given that kinetic energy and gravitational energy were exchanged and the handling of the dry bed, the conservation error of $u'h'$ and G' is good.

The Serre equations have reproduced the experimental result of Synolakis [9] well, experimentally validating the numerical methods ability to solve the Serre equations for flows over dry beds.

5. Conclusion

A second-order numerical method for the one-dimensional Serre equations with varying bathymetry was described. The method uses a FVM to solve the Serre equations in conservation law form and improves previous versions of the FVM solvers for the Serre equations [8], by using a FEM to solve for the depth-averaged horizontal velocity. The method is modified to ensure that it is well-balanced, maintaining a steady state solution over an arbitrary bathymetry and is able to handle flows over dry beds. The numerical method was validated against the lake at rest stationary solution and shown to be well-balanced. Furthermore, it reproduced forced solutions containing the wetting and drying of variable beds with second-order accuracy, affirming its ability to adequately solve the Serre equations for flows over dry beds. Finally, a numerical solution was compared to the experimental results of Synolakis [9], demonstrating the ability of the numerical method to accurately reproduce physical results involving wave run-up on a dry bed. These validation results extend those produced by other solvers of the Serre equations for flows over dry beds [4–7] by demonstrating convergence using forced solutions.

References

- [1] J.P.A. Pitt, C. Zoppou, and S.G. Roberts. Behaviour of the Serre equations in the presence of steep gradients revisited. *Wave Motion*, 76(1):61–77, 2018.
- [2] D. Lannes and P. Bonneton. Derivation of asymptotic two-dimensional time-dependent equations for surface water wave propagation. *Physics of Fluids*, 21(1):16601, 2009.
- [3] F. Serre. Contribution à l’étude des écoulements permanents et variables dans les canaux. *La Houille Blanche*, 6:830–872, 1953.
- [4] M. Tissier, P. Bonneton, F. Marche, F. Chazel, and D. Lannes. Serre Green-Naghdi modelling of wave transformation breaking and run-up using a high-order finite-volume finite-difference scheme. *Coastal Engineering Proceedings*, 1(32): 1–13, 2011.
- [5] M. Li, P. Guyenne, F. Li, and L. Xu. High order well-balanced CDG-FE methods for shallow water waves by a Green-Naghdi model. *Journal of Computational Physics*, 257(1):169–192, 2014.

- 377 [6] A. G. Filippini, M. Kazolea, and M. Ricchiuto. A flexible genuinely nonlinear
378 approach for nonlinear wave propagation, breaking and run-up. *Journal of Com-*
379 *putational Physics*, 310:381–417, 2016.
- 380 [7] J.S.A. do Carmo, J.A. Ferreira, and L. Pinto. On the accurate simulation of
381 nearshore and dam break problems involving dispersive breaking waves. *Wave*
382 *Motion*, 85:125 – 143, 2019.
- 383 [8] C. Zoppou, J. Pitt, and S. Roberts. Numerical solution of the fully non-linear
384 weakly dispersive Serre equations for steep gradient flows. *Applied Mathematical*
385 *Modelling*, 48:70–95, 2017.
- 386 [9] C.E. Synolakis. The runup of solitary waves. *Journal of Fluid Mechanics*, 185:
387 523–545, 1987.
- 388 [10] F.J. Seabra-Santos, D.P. Renouard, and A.M. Temperville. Numerical and ex-
389 perimental study of the transformation of a solitary wave over a shelf or isolated
390 obstacle. *Journal of Fluid Mechanics*, 176:117–134, 1981.
- 391 [11] A.E. Green and P.M. Naghdi. A derivation of equations for wave propagation in
392 water of variable depth. *Journal of Fluid Mechanics*, 78(2):237–246, 1976.
- 393 [12] S. Gottlieb, C. Shu, and E. Tadmor. Strong stability-preserving high-order time
394 discretization methods. *Review, Society for Industrial and Applied Mathematics*,
395 43(1):89–112, 2001.
- 396 [13] A. Kurganov, S. Noelle, and G. Petrova. Semidiscrete central-upwind schemes for
397 hyperbolic conservation laws and Hamilton-Jacobi equations. *Journal of Scien-*
398 *tific Computing, Society for Industrial and Applied Mathematics*, 23(3):707–740,
399 2002.
- 400 [14] E. Audusse, F. Bouchut, M. Bristeau, R. Klein, and B. Perthame. A fast and stable
401 well-balanced scheme with hydrostatic reconstruction for shallow water flows.
402 *Journal of Scientific Computing, Society for Industrial and Applied Mathematics*,
403 25(6):2050–2065, 2004.
- 404 [15] B. Van Leer. Towards the ultimate conservative difference scheme. IV. A second-
405 order sequel to Godunov’s method. *Journal of Computational Physics*, 32(1):
406 101–136, 1979.
- 407 [16] W.H. Press, S.A. Teukolsky, W.T. Vetterling, and B.P. Flannery. *Numerical*
408 *Recipes in C*. Cambridge University Press, London, 2nd edition, 2002.
- 409 [17] R. Courant, K. Friedrichs, and H. Lewy. On the partial difference equations of
410 mathematical physics. *IBM Journal of Research and Development*, 11(2):215–
411 234, 1967.
- 412 [18] J. Pitt. *A Second Order Well Balanced Hybrid Finite Volume and Finite Difference*
413 *Method for the Serre Equations*. Honour’s thesis, Australian National University,
414 Mathematical Sciences Institute, College of Physical and Mathematical Sciences,
415 Australian National University, Canberra, ACT 2600, Australia, 2014.

- 416 [19] A. Kurganov and G. Petrova. A second-order well-balanced positivity preserving
417 central-upwind scheme for the Saint-Venant system. *Communications in Mathe-*
418 *matical Sciences*, 5(1):133–160, 2007.